



Simultaneous dehydrogenation and hydrogenolysis of aromatic alcohols in one reaction system via visible-light-driven heterogeneous photocatalysis



Sugang Meng^{a,*}, Xiaofeng Ning^a, Susheng Chang^a, Xianliang Fu^a, Xiangju Ye^b, Shifu Chen^{a,b,*}

^a College of Chemistry and Materials Science, Huaibei Normal University, Anhui, Huaibei 235000, People's Republic of China

^b College of Chemistry and Material Engineering, Anhui Science and Technology University, Anhui, Fengyang 233100, People's Republic of China

ARTICLE INFO

Article history:

Received 29 July 2017

Revised 29 September 2017

Accepted 12 November 2017

Available online 1 December 2017

Keywords:

Visible light photocatalysis

Semiconductor CdS

Selective oxidation

Selective reduction

Mechanism

ABSTRACT

Photocatalytic selective organic transformation using photoexcited holes and electrons has attracted worldwide interest. Although extensive studies have made significant progress in dehydrogenation of alcohols, hydrogenolysis of alcohols using photoexcited electrons directly constitutes a challenge. Here, photocatalytic selective dehydrogenation and hydrogenolysis of aromatic alcohols into corresponding alkanes/ethers and aldehydes has been achieved by direct use of photoexcited electrons and holes over CdS under visible light irradiation. Compared with other popular visible-light-driven photocatalysts, Sb₂S₃, Bi₂O₃, N-doped TiO₂, Zn₃In₂S₆, g-C₃N₄, and Ce₂S₃, the sum of the yields of alkanes and aldehydes over the as-prepared CdS could reach up to 94% after reaction for 4 h. The high photoactivity and stability of CdS toward dehydrogenation and hydrogenolysis of aromatic alcohols can be ascribed to its appropriate band potentials and effective charge separation–transportation. The optimum positions are that the valence band position should be located between oxidation potentials of alcohol/aldehyde and aldehyde/oxidized aldehyde, and the conduction band position should be more slightly negative than reduction potential of alkane/alcohol. During this reaction, the dehydrogenation reaction consumes two holes and produces two protons; the hydrogenolysis process depletes two electrons and two protons. Therefore, a cooperative, cyclical, and efficient reaction system was established.

© 2017 Elsevier Inc. All rights reserved.

1. Introduction

As a green and promising technology, photocatalytic reduction and oxidation reactions, based largely on renewable solar energy and mild reaction conditions and environmentally friendly, have recently attracted extensive interest in multiple areas of scientific research, such as physics, materials, chemistry, and biology [1–4]. Recent progress in photocatalytic selective organic transformations demonstrates that this green technique can obtain diverse fine chemicals by selecting appropriate photocatalysts and finer control of reaction conditions than in conventional synthetic pathways [5–8]. Its advantages lie in its ability to avoid environmentally unfriendly heavy metal catalysts, strong chemical oxidants (e.g., Cr^{IV}, ClO⁻, and Cl₂), or dangerous reducing gas reagents (e.g., H₂ and CO) and harsh reaction conditions such as high temperature and high pressure [9–11]. It is known that selective oxidation (dehydrogenation) of alcohols is a fundamental but significant

reaction for the synthesis of fine chemicals such as aldehydes and their derivatives under O₂ [12–14]. However, a major challenge for achieving industrialization is to restrain the recombination of photogenerated electron (e⁻)–hole (h⁺) pairs and acquire high selectivity and photocatalytic efficiency [5,6].

Thus, a number of efforts have been made to design composites for inhibiting the recombination of e⁻–h⁺ pairs and improving charge transport [15–20]. More recently, we have found that photogenerated e⁻–h⁺ pairs could be separated and utilized efficaciously for simultaneous selective redox aromatic alcohols/nitrobenzene to aldehydes/aniline over a single photocatalyst, CdS [21] or CdIn₂S₄ [22], in one reaction system under visible light. It is worth noting that the activity of selective oxidation of alcohols in this cooperative photoredox system is much higher than that in single photocatalytic oxidation under O₂. This proves that the photogenerated e⁻–h⁺ pairs are separated and utilized effectively in the reaction system. The photoexcited h⁺ and e⁻ offer their own oxidizing and reducing ability and participate in the organic transformation. Consequently, in a photocatalytic reaction system, can aromatic alcohols achieve hydrogenolysis at the same time of

* Corresponding authors.

E-mail addresses: mengsugang@126.com (S. Meng), chshifu@chnu.edu.cn (S. Chen).

dehydrogenation? How about reduction of aromatic alcohols over photoexcited electrons? Up to now, only one publication [23] has reported photocatalytic dehydrogenation and hydrogenolysis of aromatic alcohols in one reaction system. In that work, semiconductor–metal photocatalysts (Pt/CdS and Pd/CdS_{0.4}Se_{0.6}) were used for sunlight-driven dehydrogenation and hydrogenolysis of benzyl alcohol into H₂ and hydrocarbons. However, Pt/CdS favored dehydrogenation over hydrogenolysis to produce H₂, whereas Pd/CdS_{0.4}Se_{0.6} favored hydrogenolysis over dehydrogenation to form toluene. It is hard simultaneously to realize photocatalytic dehydrogenation and hydrogenolysis of alcohols into corresponding alkanes and aldehydes with high selectivity in one photocatalytic reaction system. Moreover, the reaction mechanism has not been clarified up to now.

Here, photocatalytic dehydrogenation and hydrogenolysis of aromatic alcohols (R–Ph–CH₂OH, R=H, Me, OMe, and OEt) into corresponding alkanes/ethers and aldehydes have been achieved in one reaction system by direct use of photoexcited holes and electrons generated on CdS nanoparticles under visible light irradiation under N₂ (Scheme 1). The cooperative photoredox reaction not only represents an efficient, atom-economical, and versatile transformation due to the simultaneous production of easily separable aldehydes and alkanes/ethers under mild conditions, but also can develop a new approach to applying the photoexcited e[−]–h⁺ pairs and improving the separation efficiency of photogenerated carriers. For instance, the conversion of p-methoxybenzyl alcohol (pMBA) could achieve 100%, and the sum of the yields of p-methoxybenzaldehyde (pMBAD) and p-methylanisole (pMA) could reach up to 94% over the as-prepared CdS photocatalyst under visible light irradiation in only 4 h. The efficient reaction system could also be attained for selective redox of other aromatic alcohols and in different solvents. Moreover, aldehydes and ethers are important fine chemicals that are widely utilized in fragrances and pharmaceuticals and as intermediates in chemical synthesis [6–8,24,25]. Therefore, this photocatalytic reaction toward dehydrogenation and hydrogenolysis of aromatic alcohols is of great value in organic synthesis. Finally, the high photocatalytic performance (activity and stability) of CdS toward dehydrogenation and hydrogenolysis of aromatic alcohols was investigated by a series of control experiments. A possible mechanism was proposed and proved by photoluminescence (PL), reactive-species-scavenger, electron paramagnetic resonance (EPR), and isotopic tracing experiments.

2. Experimental

2.1. Materials

Cadmium nitrate (Cd(NO₃)₂·4H₂O, 99%), sodium sulfide (Na₂S·9H₂O, 98.0%), benzotrifluoride (C₆H₅CF₃, BTF, 99.0%), p-methoxybenzyl alcohol (MeOC₆H₄CH₂OH, pMBA, 98.0%), p-tolylmethanol (MeC₆H₄CH₂OH, pTMA, 98%), p-ethoxybenzyl alcohol (EtOC₆H₄CH₂OH, pEMA, 98.5%), cyclohexane (C₆H₁₂, 99.5%), methylbenzene (C₆H₅CH₃, 98%), acetonitrile (CH₃CN, 99%), phenol

(C₆H₅OH, 98.0%), triethanolamine (C₆H₁₅NO₃, 98.0%), tetrachloromethane (CCl₄, 99.5%), sodium sulfate anhydrous (Na₂SO₄, 99.0%), and commercial cadmium sulfide (CdS, 98%) were purchased from Aladdin Industrial. 5,5-Dimethyl-1-pyrroline N-oxide (DMPO, ≥97%) and 2,2,6,6-tetramethyl-1-piperidinyloxy (TEMPO, 98%) were purchased from Sigma-Aldrich. Deuterated p-methoxybenzyl alcohol MeOPhCD₂OD (98%) and MeOPhCD₂OH (98%) were purchased from Macklin. All the reagents used in the experiments were of analytical grade and without any further purification. Deionized water used in the synthesis was from local sources.

2.2. Preparation of photocatalysts

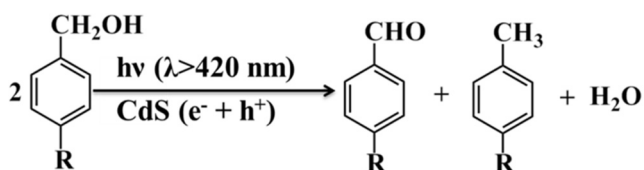
Dispersed CdS nanoparticles were prepared by a hydrothermal method. In a typical synthesis, 1.067 g of Cd(NO₃)₂·4H₂O was dissolved in 70 mL of deionized water to form a clear solution that was stirred for 30 min at room temperature, followed by the addition of 1.662 g Na₂S·9H₂O. Afterward, the mixture was stirred for 30 min, transferred to a Teflon-lined stainless steel autoclave with capacity 100 mL, and maintained at 140 °C for 24 h and at room temperature for 24 h, respectively. The obtained precipitates were washed several times with deionized water to remove possible remaining cations and anions before being fully dried at 353 K in an oven. The obtained sample is denoted as CdS-Hy. For comparison, CdS-Pr (CdS-pristine) was also prepared by the same procedure, except for being at ambient temperature (20 °C) instead of 140 °C. The reference samples Sb₂S₃ [26], N-doped TiO₂ (N-TiO₂) [27], Zn₃In₂S₆ [28], Ce₂S₃ [29], g-C₃N₄ [30], and Bi₂O₃ [31] were prepared by procedures reported elsewhere.

2.3. Characterization

The phases of CdS samples were analyzed using a Bruker D8 Advance X-ray diffractometer (XRD) using CuKα radiation at 40 kV and 40 mA in the 2θ range from 10° to 80° at a scan rate of 0.05° per second. The optical properties of the sample were characterized by UV–vis diffuse reflectance spectroscopy (DRS) using a UV–vis spectrophotometer (Cary 500, Varian Co.), in which BaSO₄ was used as the internal reflectance standard. Scanning electron microscopy (SEM) and energy-dispersive X-ray spectroscopy (EDX) were employed to determine the morphology and elemental composition of the sample on an FEI Nova NANOSEM 450 spectrophotometer. Transmission electron microscopy (TEM) images and high-resolution TEM (HRTEM) images were obtained using a FEI Tecnai G² F20 S-Twin. X-ray photoelectron spectroscopy (XPS) was carried out on a Thermo Scientific ESCA Lab250 spectrometer, which consists of a monochromatic AlKα (1486.6 eV) beam as the X-ray source, a hemispheric analyzer, and a sample stage with multiaxial adjustability to obtain the surface composition of the sample. All of the binding energies were calibrated by the C1s peak at 284.6 eV. Photoluminescence (PL) emission spectra were recorded on a JASCO FP 6500 type fluorescence spectrophotometer with an excitation wavelength of 420 nm at room temperature. Electron paramagnetic resonance (EPR) spectra were measured on a Bruker A300 EPR spectrometer and the same light source as that for the photocatalytic reaction. The Brunauer–Emmett–Teller (BET) specific surface area (S_{BET}) of the sample powders was analyzed by nitrogen adsorption–desorption in a Micromeritics ASAP 2020 apparatus.

2.4. Photoelectrochemical performance

All electrochemical experiments were performed with a CHI 660E electrochemical workstation (CHI Instruments, USA). The photocurrent, electrochemical impedance spectroscopy (EIS), open



Scheme 1. Photocatalytic dehydrogenation and hydrogenolysis of aromatic alcohols into corresponding alkanes and aldehydes in one reaction system by direct use of photoexcited holes (h⁺) and electrons (e[−]) generated on CdS under visible light irradiation.

circuit potential, and Mott–Schottky (M-S) experiments were carried out using a conventional three-electrode cell (an as-prepared CdS electrode (50 × 50 mm, ITO/CdS) as the working electrode, a Pt wire as the counter electrode, and an Ag/AgCl electrode as the reference electrode). The electrolyte for photocurrent, open circuit potential, and M-S experiments was 0.1 mol/L Na₂SO₄ solution. The electrolyte for EIS was a 0.1 M KCl aqueous solution containing 0.01 M K₃[Fe(CN)₆]-K₄[Fe(CN)₆]. Cyclic voltammetry (CV) was carried out by sweeping at 0.05 V s⁻¹ in CH₃CN/0.1 mol/L LiClO₄/0.2 mmol L⁻¹ pMBA solution. A glass carbon disk, a platinum wire, and an Ag/AgCl electrode were used as the working, counter, and reference electrodes, respectively.

2.5. Evaluation of photocatalytic activity

Photocatalytic selective oxidation and reduction of aromatic alcohols were performed as follows. For oxidation and reduction of p-methoxybenzyl alcohol (pMBA), portions of pMBA (2.55 × 10⁻² mol/L) and 0.1 g catalyst were added to benzotrifluoride (BTF, 15 mL). The mixture was put into a self-designed photochemical 100 mL reactor, which was filled with molecular nitrogen at a pressure of 0.1 MPa and stirred for 30 min in the dark to ensure adsorption–desorption equilibrium between the photocatalyst and the reactants before irradiation. A 300-W Xe arc lamp (PLS-SXE 300, Beijing Perfectlight) equipped with filters to cut off light of wavelength < 420 nm was employed as the irradiation source. Because of continuous cooling with refrigerated circulating water (10 °C), a heating effect can be excluded. After the illumination reaction, the mixture was centrifuged to completely remove the catalyst particles. The remaining solution was analyzed with gas chromatography (GC, Fuli 9790, China) and gas chromatography–mass spectrometry (GC–MS, Agilent Technologies, 7890A, Waldbronn, Germany). Conversion of pMBA and yield and selectivity for p-methoxybenzaldehyde (pMBAD)/p-methyl anisole (pMA) were calculated as follows:

$$\text{Conversion(\%)} = [(C_0 - C_{\text{pMBA}})/C_0] \times 100$$

$$\text{Yield(\%)} = [C_{\text{pMBAD(or pMA)}}/C_0] \times 100$$

$$\text{Selectivity(\%)} = [C_{\text{pMBAD(or pMA)}}/(C_0 - C_{\text{pMBA}})] \times 100,$$

where C_0 is the initial concentration of pMBA, and C_{pMBA} and $C_{\text{pMBAD(or pMA)}}$ are the concentrations of the substrate pMBA and the corresponding pMBAD (or pMA), respectively, at a certain time after the photocatalytic reaction.

The cycling experiments were performed as follows to evaluate the reusability of CdS-Hy. After each run of the photocatalytic reaction, the sample was centrifuged, washed three times with BTF, dried at 60 °C, and used for the next run under identical conditions. Due to the loss of sample inevitable in the collection process, a small amount of fresh sample was added to maintain a weight of 0.1 g for each run.

3. Results and discussion

The well-crystallized CdS-Hy nanoparticles with cubic phase were synthesized by a simple hydrothermal method. As shown in Fig. 1a, all the diffraction peaks of its X-ray diffraction (XRD) pattern can easily be indexed to the pure cubic phase of CdS (JCPDS No. 10-0454). The peaks at 2θ values of 26.5°, 30.8°, 43.9°, 52.1°, 64.0°, 70.3°, and 72.8° are indexed to the (1 1 1), (2 0 0), (2 2 0), (3 1 1), (4 0 0), (3 3 1), and (4 2 0) crystal planes of cubic CdS, respectively. To further investigate the surface element compositions and the chemical state of the as-prepared CdS-Hy sample, X-ray photoelectron spectroscopy (XPS) measurements were car-

ried out. Fig. 1b presents a typical XPS survey spectrum of CdS-Hy. Cd, S, O, and C are observed and the corresponding photoelectron peaks appear at binding energies of 405.1 (Cd3d), 161.4 (S2p), 530.5 (O1s), and 284.6 eV (C1s), respectively. The peaks for C and O are probably ascribable to the graphite conductive adhesive or the absorbed gaseous molecules. The binding energies corresponding to Cd3d_{5/2} and Cd3d_{3/2} are 405.1 and 411.9 eV, respectively (Fig. 1c), indicative of Cd²⁺ in CdS. The 6.8 eV difference between the binding energies of the Cd3d_{5/2} and Cd3d_{3/2} peaks is also characteristic of Cd²⁺ states [32,33]. As shown in Fig. 1d, binding energies of S2p for S2p_{3/2} and S2p_{1/2} are determined to be about 161.4 and 162.5 eV, respectively, demonstrating a normal state of S²⁻ in the CdS-Hy sample [34]. Furthermore, the atomic ratio of Cd to S is almost 1:1, which is in good agreement with the nominal atomic composition of CdS.

The SEM image in Fig. 2a reveals that CdS-Hy consists of nanoparticles with sizes from ca. 10–15 nm. Energy-dispersive X-ray spectroscopy (EDX) analysis confirms the elemental composition of the as-prepared CdS-Hy (Fig. 2b). It indicates the presence of the elements of Cd and S. As shown in the TEM (Fig. 2c) and high-resolution TEM (HRTEM) (Fig. 2d) images, the sizes of dispersed CdS-Hy nanoparticles are less than 20 nm and single particles exhibit good crystallization. The lattice fringes with *d*-spacings of 0.336 and 0.175 nm are assigned to the strong reflection of the (1 1 1) and (3 1 1) planes, which is in line with the XRD results.

In addition, CdS-Hy has visible light absorption capability (up to 540 nm), corresponding to ca. 2.32 eV of the band gap energy (Fig. 3a), and the flat-band potential of CdS-Hy was determined to be approximately -0.69 V vs. Ag/AgCl (Fig. 3b). Therefore, the conduction band (CB) and valence band (VB) positions of CdS-Hy are -0.49 V and 1.83 V vs. NHE, respectively (see details in the Electronic Supplementary Information). On the other hand, for conversion of p-methoxybenzyl alcohol (pMBA) into p-methoxybenzaldehyde (pMBAD) and p-methyl anisole (pMA) as an example, the voltammogram of pMBA (Fig. 3c) exhibits an irreversible curve and possesses two oxidative potentials. The first oxidative potential (ca. 1.36 V vs. Ag/AgCl) is assigned to pMBA/pMBAD; the second oxidative potential (ca. 1.81 V vs. Ag/AgCl) belongs to pMBAD/oxidized pMBAD. Consequently, as shown in Fig. 3d, we can conclude that the CB of CdS-Hy is more negative than the reductive potential of pMBA, and the VB is more positive than the oxidative potential of pMBA/pMBAD, but is not more positive than pMBAD/oxidized pMBAD. Therefore, a green and mild photocatalytic process for selective dehydrogenation and hydrogenolysis of pMBA would be achieved over CdS-Hy in one reaction system with high selectivity.

The photocatalytic performance of the CdS-Hy sample was evaluated by selective dehydrogenation and hydrogenolysis of pMBA under visible light irradiation ($\lambda > 420$ nm). First, the effect of the amount of CdS-Hy on the photocatalytic activity was studied. As shown in Fig. S1 in the Electronic Supplementary Information, the optimized amount of CdS-Hy is 0.1 g. Therefore, 0.1 g of CdS-Hy was used in the following photocatalytic activity tests. To further probe into the details of activity and selectivity distribution of the product for dehydrogenation and hydrogenolysis of pMBA, we have determined a time-online reaction profile with the irradiation time (Fig. 4a). It can be seen that the activity of CdS-Hy in terms of conversion of pMBA and yields of pMBAD and pMA gradually increases with increased reaction time. After irradiation for 1 h, the conversion of pMBA could reach up to 61.6%. However, negligible photoactivities are observed in the blank experiments (without catalyst or no light irradiation). In addition, the conversion of pMBA and yields of pMBAD and pMA do not increase with rising temperature (Fig. S2). These confirm that the redox reactions are primarily driven by a photocatalytic process. It should be noted that, after only 4 h, the conversion of pMBA was already 100%, and

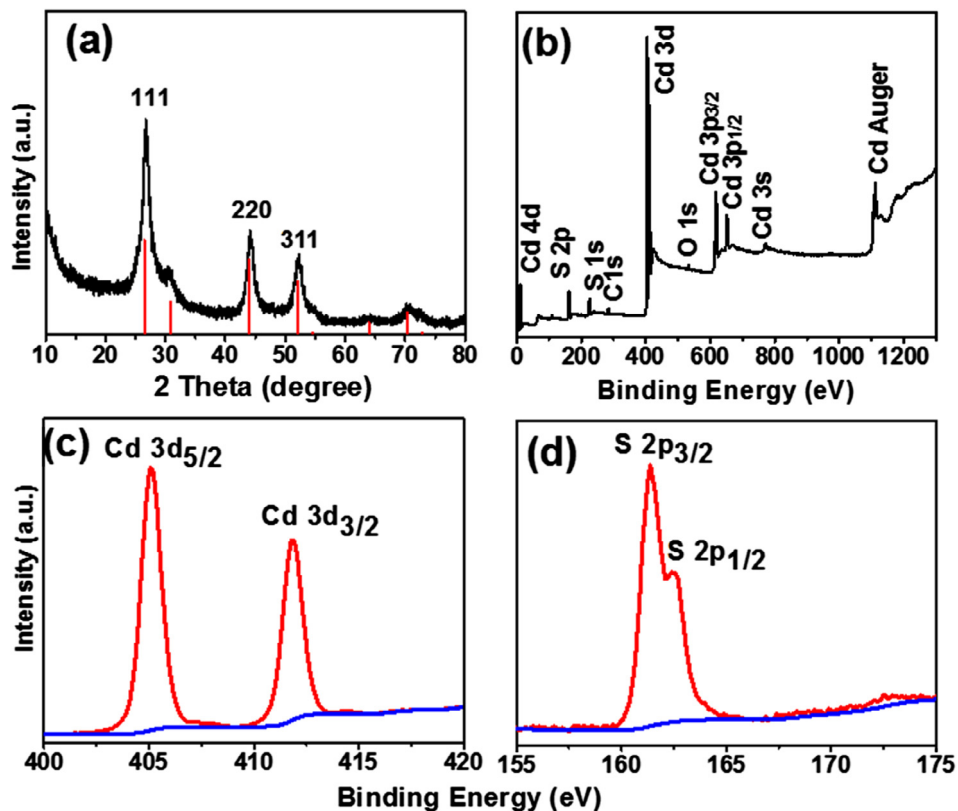


Fig. 1. (a) XRD pattern of CdS-Hy, (b) XPS survey spectrum of CdS-Hy, and high-resolution spectra of (c) Cd3d and (d) S2p.

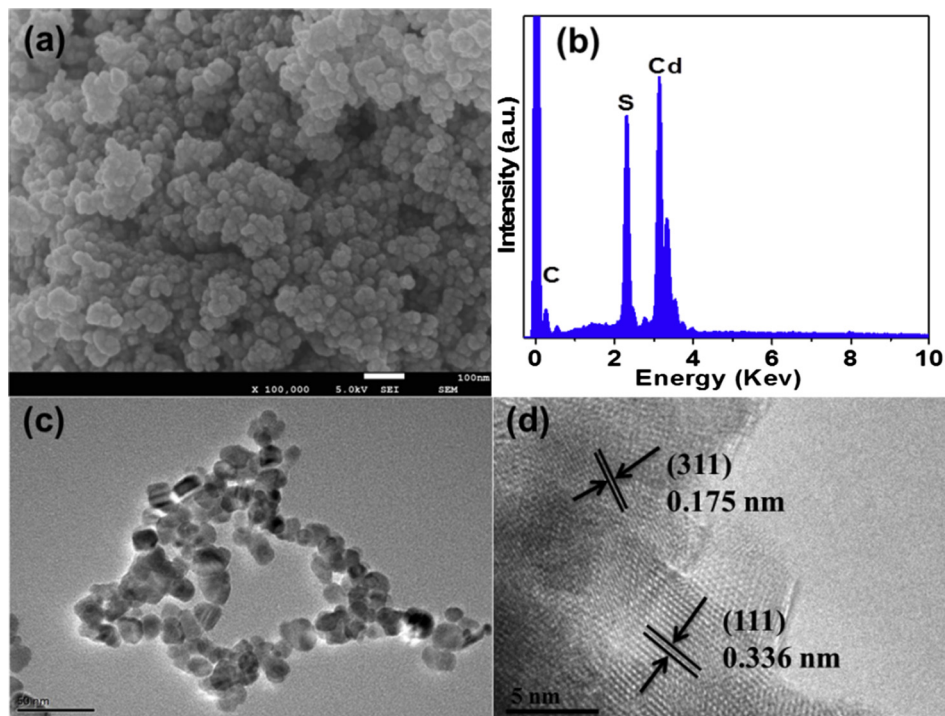


Fig. 2. (a) SEM image, (b) EDX pattern, and (c) TEM and (d) HRTEM images of CdS-Hy.

the sum of the yields of pMBAD (52.3%) and pMA (41.7%) reached 94%. Moreover, the linear correlation of $\ln(C/C_0)$ (C_0 and C are the concentration of pMBA before and after illumination, respectively) and time profile suggest pseudo-first-order reaction kinetics for

this reaction (Fig. 4b), and the apparent reaction rate constant (k) is 1.1672 h^{-1} . This indicated that pMBA could be efficiently disproportionated to pMBAD and pMA over CdS-Hy under mild reaction conditions. Specifically, the photocatalytic products were analyzed

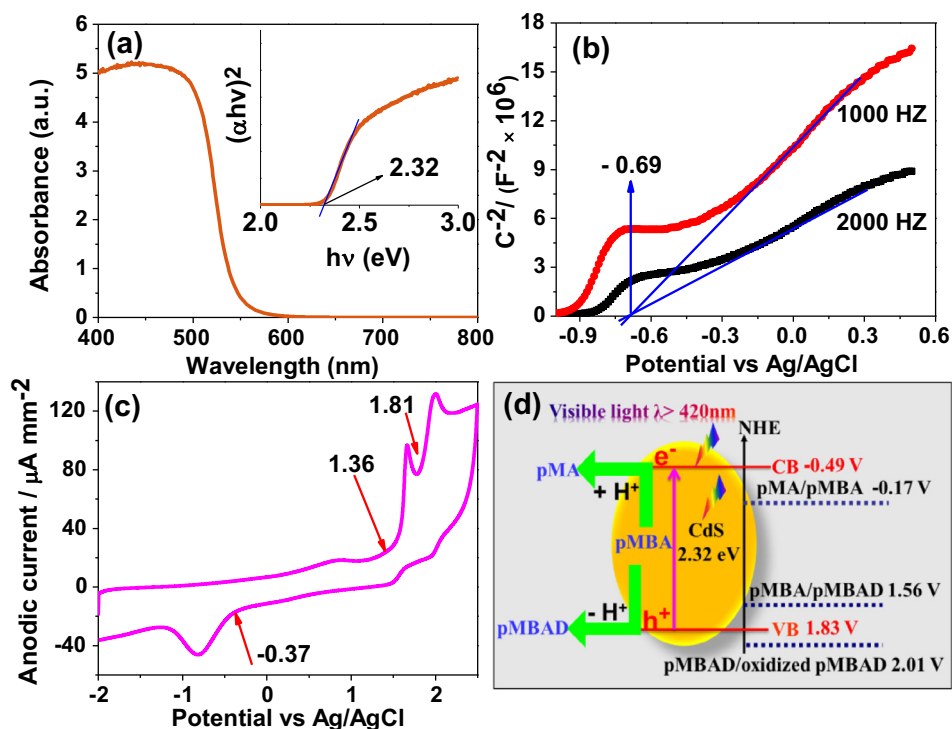


Fig. 3. (a) UV-vis DRS and band-gap energy (inset) and (b) Mott-Schottky plots of CdS-Hy. (c) The cyclic voltammogram of pMBA. (d) Schematic diagram showing the band positions of CdS-Hy, redox potentials of pMBA, and selective redox of pMBA over CdS-Hy under visible light irradiation (pMBA: p-methoxybenzyl alcohol, pMBAD: p-methoxybenzaldehyde, pMA: p-methyl anisole).

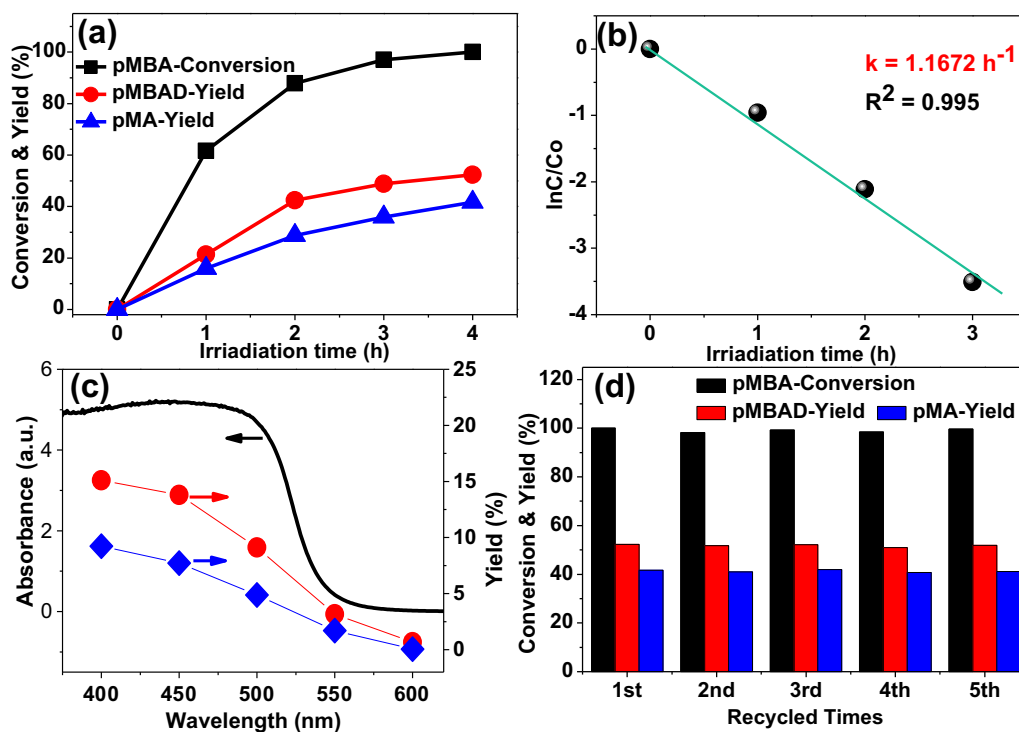


Fig. 4. (a) Time-online photocatalytic selective reduction-oxidation of pMBA activity and (b) the kinetics of pMBA conversion over CdS-Hy under visible-light irradiation. (c) Wavelength-dependent pMBAD and pMA yields with the CdS-Hy under monochromatic light irradiation. (d) Recycled testing of photocatalytic activity of CdS-Hy toward the selective oxidation and reduction pMBA under visible light irradiation for 20 h (pMBA: p-methoxybenzyl alcohol, pMBAD: p-methoxybenzaldehyde, pMA: p-methyl anisole).

by gas chromatography (GC) and gas chromatography-mass spectroscopy (GC-MS) (Figs. S3 and S4). This does verify that CdS-Hy can dehydrogenate pMBA to pMBAD and hydrogenate pMBA to

pMA in one reaction system. Furthermore, the pMBAD and pMA generation activities match the CdS-Hy optical absorption spectrum in Fig. 4c, clearly demonstrating that the dehydrogenation

and hydrogenolysis reaction is truly driven by a photocatalysis process on CdS-Hy.

In addition to high activity, stability is another important characteristic of a catalyst for industrialization. To test the photostability and reusability of CdS-Hy during photocatalytic reactions, cycling experiments were also carried out. As shown in Fig. 4d, the photocatalytic activity of CdS-Hy shows almost no deactivation even after five consecutive cycles. Additionally, the used CdS-Hy had an XRD pattern identical to that of the fresh CdS-Hy (Fig. S5), and the amount of Cd²⁺ in the reacted suspension detected by ICP-MS was only 10.3 ppb. Therefore, it could be demonstrated that the as-synthesized CdS-Hy is a stable photocatalyst for visible-light-driven selective dehydrogenation and hydrogenolysis of pMBA. It should be noted that reusability of a catalyst is one of the great advantages of heterogeneous photocatalysis, while catalysts can only be used once for synthesis of organics in traditional homogeneous catalysis.

Moreover, pMA and pMBAD can also be formed in nonfluorinated solvents (such as cyclohexane (C₆H₆) and methylbenzene (PhCH₃)), and CdS-Hy also functions as a photocatalyst with high activity and high selectivity for dehydrogenation and hydrogenolysis of other aromatic alcohols (p-tolylmethanol (pTMA), p-ethoxybenzyl alcohol (pEMA), and benzyl alcohol (BA)), as shown in Figs. S6 and FS7. These results strongly suggest that CdS-Hy can be used as an efficient visible-light-driven photocatalyst for the selective dehydrogenation and hydrogenolysis of aromatic alcohols under mild reaction conditions.

Then why can CdS-Hy display high activity and stability for dehydrogenation and hydrogenation reactions of aromatic alcohols? What are the main factor and the reaction mechanism? How about other photocatalysts? It is known that the performance of photocatalysts is greatly limited by two conditions [35,36]: (1) the redox potential of reactants should be located between the VB and CB of the photocatalyst; (2) the photoexcited charges should be separated, transported, and utilized effectively.

A series of experiments were carried out to try to address the above questions. First, to clarify the roles of redox potentials of

photocatalysts in the selective redox of pMBA into pMA and pMBAD, several visible-light-driven photocatalysts (Sb₂S₃ [26], Bi₂O₃ [31], N-doped TiO₂ (N-TiO₂) [27], Zn₃In₂S₆ [28], g-C₃N₄ [30], and Ce₂S₃ [29]) were employed to hydrogenate and dehydrogenate pMBA. From Figs. S8 and S9, it can be seen that the XRD patterns of the as-prepared Sb₂S₃, N-TiO₂, Zn₃In₂S₆, Ce₂S₃, g-C₃N₄, and Bi₂O₃ are in good agreement with the standard XRD patterns of Sb₂S₃ (JCPDS 42-1393), N-TiO₂ (JCPDS 65-5714), Zn₃In₂S₆ (JCPDS 65-4003), Ce₂S₃ (JCPDS 43-0800), g-C₃N₄ (JCPDS 87-1526), and Bi₂O₃ (JCPDS 65-2366), respectively. Moreover, their morphologies are in line with the previous reports [26–31]. These semiconductors are representative photocatalysts and could be classified as six types on the basis of their CB/VB positions (denoted as φ_{CB} and φ_{VB} , respectively) and the redox potentials of pMA/pMBA, pMBA/pMBAD, and pMBAD/oxidized pMBAD (denoted as $\varphi_{pMA/pMBA}$, $\varphi_{pMBA/pMBAD}$, and $\varphi_{pMBAD/oxidized\ pMBAD}$, respectively). As shown in Fig. 5a, we define Sb₂S₃ as type I with φ_{CB} less negative than $\varphi_{pMA/pMBA}$ and φ_{VB} more positive than $\varphi_{pMBA/pMBAD}$, but less positive than $\varphi_{pMBAD/oxidized\ pMBAD}$. Bi₂O₃ is defined as type II with φ_{CB} less negative than $\varphi_{pMA/pMBA}$ and φ_{VB} more positive than $\varphi_{pMBAD/oxidized\ pMBAD}$. N-TiO₂ is defined as type III with φ_{CB} more negative than $\varphi_{pMA/pMBA}$ and φ_{VB} more positive than $\varphi_{pMBAD/oxidized\ pMBAD}$. CdS-Hy, CdS-Pr, and CdS-C are defined as type IV with φ_{CB} more negative than $\varphi_{pMA/pMBA}$ and φ_{VB} more positive than $\varphi_{pMBA/pMBAD}$, but less positive than $\varphi_{pMBAD/oxidized\ pMBAD}$. Zn₃In₂S₆ and g-C₃N₄ are defined as type V with φ_{CB} much more negative than $\varphi_{pMA/pMBA}$ and φ_{VB} more positive than $\varphi_{pMBA/pMBAD}$, but less positive than $\varphi_{pMBAD/oxidized\ pMBAD}$. Ce₂S₃ is defined as type VI with φ_{CB} more negative than $\varphi_{pMA/pMBA}$ and φ_{VB} less positive than $\varphi_{pMBA/pMBAD}$. Fig. 5b summarizes the overall conversion rates of pMBA and the yields of pMA and pMBAD over nine photocatalysts under visible irradiation for 4 h. It is easy to get the following results: (1) pMBAD can be obtained over the photocatalysts (Sb₂S₃, Bi₂O₃, N-TiO₂, CdS-Hy, CdS-Pr, CdS-C, Zn₃In₂S₆, and g-C₃N₄) with φ_{VB} more positive than $\varphi_{pMBA/pMBAD}$, and the photocatalysts with φ_{VB} less positive than $\varphi_{pMBAD/oxidized\ pMBAD}$ exhibit higher dehydrogenation activity (yield of pMBAD) than the photo-

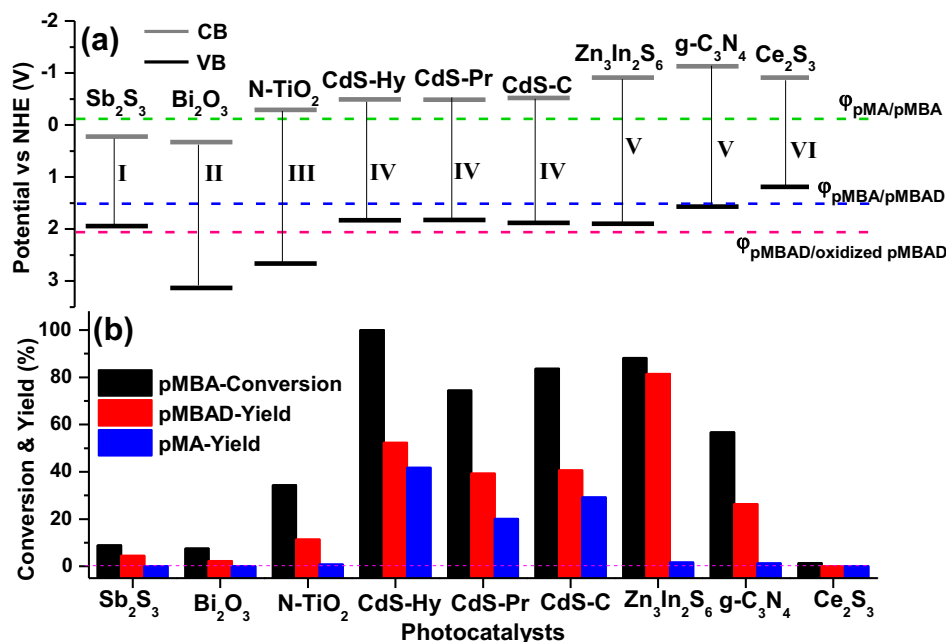


Fig. 5. (a) The relationship between the band positions of different photocatalysts and the redox potentials of pMBA and pMBAD. (b) The activity of different photocatalysts for photocatalytic oxidation and reduction of pMBA under visible light irradiation for 4 h (pMBA: p-methoxybenzyl alcohol, pMBAD: p-methoxybenzaldehyde, pMA: p-methyl anisole).

catalysts with more positive φ_{VB} than $\varphi_{pMBAD/oxidized\ pMBAD}$. For instance, more pMBAD could be produced over type I than type II, and over types IV and V than type III. This is because that much more positive φ_{VB} could immoderately oxidize pMBA, which is in line with previous reports that benzyl alcohol could be oxidized to yield benzoic acid or carbon dioxide over TiO_2 [4,11]. (2) pMA can only be synthesized over the photocatalysts (N-TiO₂, CdS-Hy, CdS-Pr, CdS-C, Zn₃In₂S₆, and g-C₃N₄) with φ_{VB} more positive than $\varphi_{pMBA/pMBAD}$ and φ_{CB} more negative than $\varphi_{pMA/pMBA}$, and more pMA could be produced over type IV than types III and V. (3) pMBAD and pMA would not be formed over the photocatalyst (Ce₂S₃) with φ_{VB} less positive than $\varphi_{pMBA/pMBAD}$ and φ_{CB} more negative than $\varphi_{pMA/pMBA}$. In this cooperative photoredox reaction, photogenerated holes and electrons contribute to dehydrogenation and hydrogenolysis, respectively. The band positions of the photocatalyst are criteria for dehydrogenation and hydrogenolysis of pMBA into pMA and pMBAD. On the basis of these results, it can be concluded that (1) the optimum positions are that φ_{VB} should be located between $\varphi_{pMBA/pMBAD}$ and $\varphi_{pMBAD/oxidized\ pMBAD}$ and φ_{CB} should be more negative than $\varphi_{pMA/pMBA}$ but not more negative than -0.91 V; (2) photocatalytic hydrogenation of pMBA is triggered after dehydrogenation of pMBA.

Generally, during photocatalysis, the photocatalytic activity of a photocatalyst could be influenced by many factors such as crystal structure, specific surface area, light absorption, band positions, and charge transportation and separation, among which charge transportation and separation is widely recognized as the most crucial factor. If we try to perform a fair evaluation between charge separation–transportation and the performance of photocatalysts, the other factors must be excluded. CdS-Pr was prepared as a representative for that reason: raw materials and crystal structure of CdS-Pr and CdS-Hy are the same (Fig. S10); their morphology, band gap energy (light absorption), and band positions (φ_{VB} and φ_{CB}) are very close (Figs. S10 and S11 and Fig. 5a); the surface area of CdS-Hy (22.9 m²/g) is not greater than that of CdS-Pr (53.6 m²/g)

(Fig. S12). That is, these parameters would not play the main role in influencing photocatalytic activity. However, their crystal structure (hexagonal CdS, JCPDS 41-1049), morphology (big particles), and surface area (10.3 m²/g) of CdS-C (Fig. S13) are different from those of CdS-Hy. It is hard to identify the differences (crystal phase, surface area, and other parameters) in activity between CdS-Hy and CdS-C that would contribute to the enhanced activity. Consequently, photoelectrochemical measurements were performed to probe into the separation and lifetime of photoinduced electron–hole pairs over CdS-Hy and CdS-Pr, which have a crucial role in achieving high photocatalytic efficiency [35–43]. Fig. 6a shows the transient photocurrent responses of CdS-Hy and CdS-Pr. It is clear that the intensity of the photocurrent follows the same order as the photocatalytic performance: CdS-Hy > CdS-Pr. The higher photocurrent indicates more effective separation and a longer lifetime of photogenerated electron–hole pairs over CdS-Hy [37,38]. Fig. 6b exhibits the Nyquist plots of CdS samples. The semicircle at high frequency corresponds to the capacitance and the resistance of the solid-state interface layer, which is formed in the highly charged state and resulted from the passivation reaction between the electrolyte and the surface of the electrode; the charge transfer resistance corresponds to the second semicircle at medium frequency. In the low-frequency region, the Warburg impedance is usually presented by a straight sloping line [39,40]. In the medium- and low-frequency regions, both semicircles of CdS-Hy are smaller than those of CdS-Pr, which implies a decrease in the charge transfer resistance on the surface [41–43]. Open circuit photovoltage decay (OCPD) measurement can be utilized to assess the lifetime of photoelectrons and evaluate the recombination rate of the photogenerated electron–hole pairs by turning off the light first in the steady state and monitoring the photovoltage (Voc) decay with time [41]. Generally, the higher Voc, the longer the electron lifetime. When the illumination is switched off, the Voc decays sharply because of electron recombination [42]. As displayed in Fig. 6c, the Voc decay rate of CdS-Hy is lower than that of

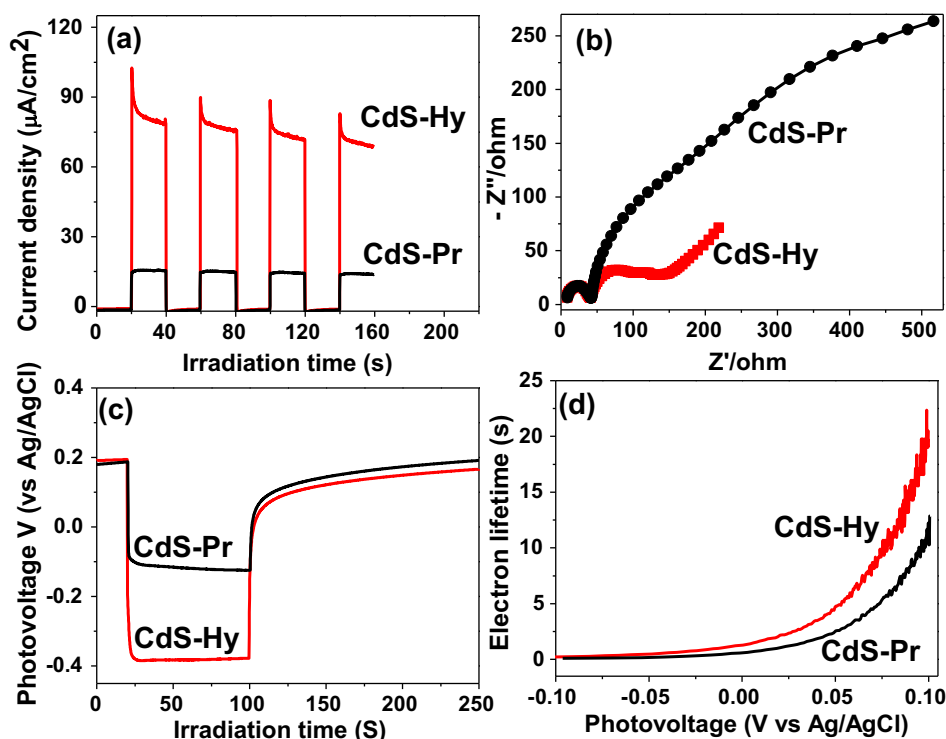


Fig. 6. (a) Transient photocurrent responses, (b) electrochemical impedance spectroscopy (EIS) Nyquist plots of the samples under visible light irradiation, (c) illuminated open circuit potential, and (d) electron lifetime determined from the decay of open circuit potential in the dark.

CdS-Pr, revealing slower recombination of the photogenerated charge carriers. The photoelectron lifetime (τ_n) was calculated by the formula $\tau_n = (k_B T/e) (dV_{OC}/dt)^{-1}$ [43]. k_B , e , T , and t are Boltzmann's constant (1.3806×10^{-23} J/K), the charge of one electron (1.602×10^{-19} C), the temperature (298.15 K), and time, respectively. As shown in Fig. 6d, the τ_n of CdS-Hy is longer than that of CdS-Pr. A longer τ_n suggests a lower electron recombination rate and more electrons surviving from the back reaction; thus, it can improve photocatalytic activity. In a word, the transient photocurrent responses, the Nyquist plots, and the open circuit photovoltage decay measurement all indicated that CdS-Hy displayed a more effective separation and longer lifetime of photogenerated electron-hole pairs than CdS-Pr. These all demonstrate that the hydrothermal synthesis of dispersed CdS nanoparticles with high crystallinity is a simple and effective method for obtaining high photocatalytic efficiency.

Photoluminescence (PL) technique was applied to detect charge-carrier recombination and utilization [44,45]. As shown in Fig. 7a, when CdS-Hy is coupled with BTF and pMBA, the PL intensity will be significantly quenched, indicating that the recombination of photogenerated electron-hole pairs over CdS-Hy in BTF solvent with reactants is mostly inhibited. The obvious PL intensity gap between CdS+BTF with and without pMBA demonstrates that the photogenerated electron and hole could be effectively trapped by pMBA, which contributes to dehydrogenation and hydrogenolysis reactions in one synergetic reaction system. Therefore, CdS-Hy displayed photostability and reusability for photocatalytic selective transformation of pMBA under visible light.

Then the trapping experiments were performed to reveal the role of the photogenerated electrons and holes (Fig. 7b). In the experiment, CCl_4 is chosen as a scavenger for trapping photogenerated electrons [46,47]. When 5 μ L CCl_4 was added into the reaction system, the yield of pMA decreased obviously, implying that the photogenerated electrons are the major reductive species for the selective hydrogenation of pMBA into pMA. Simultaneously, the yield of pMBAD increased, suggesting that the trapping of photogenerated electrons with CCl_4 could benefit the photogenerated holes inducing selective dehydrogenation of pMBA to pMBAD. When CCl_4 addition was continued to 10 μ L, it was found that the yield of pMA continued declining, and the yield of pMBAD increased to 83.5%, which indicates that CCl_4 can efficiently trap photogenerated electrons, and photogenerated electrons play a leading role in reducing pMBA in the reaction system. TEA (triethanolamine) is selected as a scavenger for trapping photogenerated holes [48,49]. When 2 μ L TEA was added into the reaction system, the yields of pMBAD and pMA both decreased; when the

amount of TEA was increased to 5 μ L, it was found that the yields of pMBAD and pMA continued decreasing, which indicates that TEA could effectively capture photogenerated holes, and the decrease of the yield of pMA could be caused by the decrease of dehydrogenation activity. This may be caused by the fact that protons are produced in the dehydrogenation of pMBA and are necessary for reduction of pMBA to pMA. This result is in line with the above analysis (Fig. 5). In the coupled reaction system, photocatalytic hydrogenation was triggered after oxidation of pMBA. Thus, when phenol was added to the system to provide protons, the yield of pMA could be improved, which illustrates that protons do play a vital role in hydrogenating pMA in this reaction system.

To investigate the process of protons being dehydrogenated from pMBA and then hydrogenated on pMBA, isotopic tracing experiments were carried out (Fig. S2). Hydrogen atoms of O-H and α C-H were replaced with deuteriohydrogen atoms. When MeOPhCH₂OD was employed, the dehydrogenation and hydrogenolysis products are MeOPhCHO and MeOPhCH₂D, respectively, while for MeOPhCD₂OH, the dehydrogenation product is MeOPhCDO and the hydrogenolysis product is mainly MeOPhCD₂-H. This suggested that O-H and α C-H dehydrogenation and α C-O hydrogenolysis indeed occur in the photocatalytic reactions. In addition, there is less deuterated pMA than hydrogen-bearing pMA, implying that the activation of an α C-H is the slow step in the dehydrogenation and hydrogenolysis of pMBA. This is in line with the previous reports [15,16].

To gain better insight into the nature of adsorption, surface-sensitive FTIR experiments were performed for pMBA on the CdS-Hy surface in the manner of a previous study [50]. As shown in Fig. S14, the signals of pMBA in BTF solution on the CdS-Hy surface in FTIR were obvious. This indicates that pMBA can be adsorbed on the CdS-Hy surface. The result is in line with the above-reported work (aliphatic primary alcohols with short chains could be adsorbed onto the Pt/TiO₂ surface) [50]. However, aliphatic primary alcohols with short chains were dehydrogenated into aldehydes in poor selectivity. The seemingly inconsistent results may be caused by the different reaction system (photocatalyst and reaction substrates). It is known that TiO₂ showed low selectivity for selective oxidation of aromatic alcohols to aromatic aldehydes under UV irradiation because of its high oxidation ability (the potential of the photogenerated holes in the valence band is 2.7 V) [36,51]. For instance, Zhao and co-workers [51] developed a coupled system of dye-sensitized TiO₂ and TEMPO that could effectively oxidize aromatic alcohols to aromatic aldehydes using oxygen and visible light, which avoided the generation of strong and nonselective oxidant photogenerated holes and hydroxyl rad-

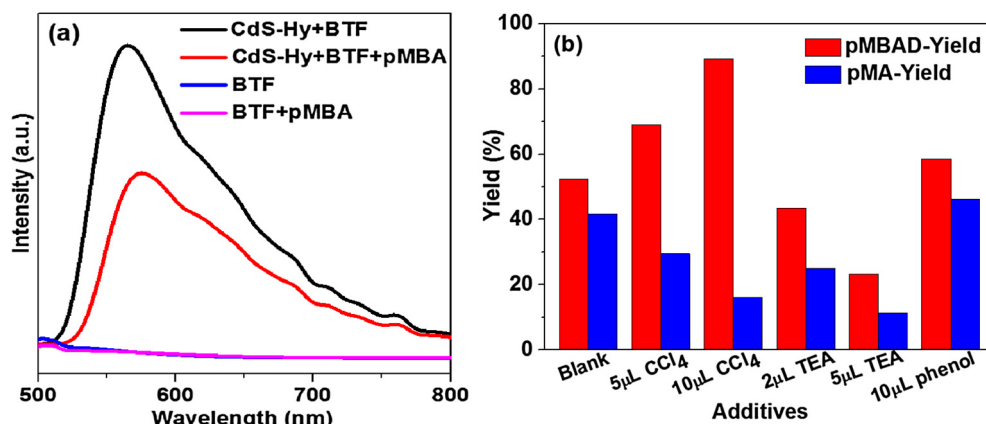
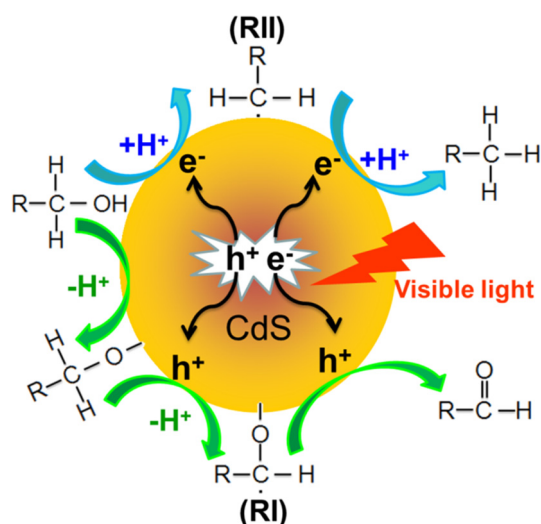


Fig. 7. (a) Photoluminescence (PL) spectra of CdS-Hy under different conditions (excitation wavelength 420 nm). (b) Yields of pMBAD and pMA over CdS-Hy by adding different additives under visible light for 4 h (BTF: benzotrifluoride, pMBA: p-methoxybenzyl alcohol, pMBAD: p-methoxybenzaldehyde, pMA: p-methyl anisole).

icals. Moreover, the selectivity of photocatalytic oxidation of alcohols is highly dependent on the position of the valence band of photocatalysts. In this work, the potential of the photogenerated holes in the valence band of CdS-Hy is 1.83 V, which is much lower than that of TiO₂, and importantly is located between the oxidative potentials of pMBA/pMBAD (1.56 V) and pMBA/oxidized pMBAD (2.01 V). Therefore, the oxidation ability of CdS-Hy is much lower than that of TiO₂, but is strong enough to oxidize pMBA into pMBAD and cannot further oxidize pMBAD. Therefore, pMBA adsorbed on the surface could be oxidized into pMBAD and avoid over oxidation, resulting in high selectivity of CdS-Hy.

Therefore, based on the above results and analysis, a possible mechanism was proposed (Scheme 2). First, CdS-Hy was excited by visible light and produced photoexcited electrons and holes. A pMBA molecule was adsorbed onto the surface of CdS-Hy to form an alkoxide anion via a deprotonated process; the alkoxide anion was then reacted with a photogenerated hole and deprotonated to form a carbon radical (RI), which further reacted with one photogenerated hole to form a pMBAD molecule. On the other hand, pMBA captured one proton and one photogenerated electron to form an intermediate carbon radical (RII) by a dehydration process; the carbon radical (RII) was then reduced by one proton and one



Scheme 2. Proposed reaction processes for the photocatalytic selective reduction-oxidation of aromatic alcohols over CdS-Hy under visible light irradiation (R = MeOPh-, MePh-, Ph-, and EtOPh-).

electron to produce a pMA molecule. In this cooperative photoredox reaction, the dehydrogenation reaction consumes two holes and produces two protons; the hydrogenolysis process depletes two electrons and two protons. Therefore, a cyclic and efficient reaction system was established.

To ascertain the formation of RI and RII, we monitored their signals in the reaction system by electron paramagnetic resonance (EPR) spectroscopy. DMPO (5,5-Dimethyl-1-pyrroline N-oxide) and TEMPO (2,2,6,6-Tetramethyl-1-piperidinyloxy) are typical probe molecules for trapping carbon radicals and electrons (e⁻) [52–54]. As shown in Fig. 8a, when both TEMPO and DMPO were added into the reaction system, the EPR spectrum exhibits a stable triplet signal with intensity 1:1:1 at $t = 0$ min (labeled by *). The triplet signal intensity was decreased with irradiation time, indicating that the electrons are produced from photoexcited CdS-Hy and can be trapped effectively by TEMPO. While irradiated by visible light, the EPR spectrum presents a new characteristic six peaks (labeled by ♠, $a_N = 14.8$ G, $a_H = 22.4$ G), indicating that a carbon-centered radical was trapped by DMPO. In this process, the electrons are trapped by TEMPO, resulting in no formation of RII. Therefore, the six peaks in Fig. 8a are reasonably assigned to an adduct of DMPO formed by trapping RI. On the other hand, with only addition of DMPO, the six peaks in Fig. 8b exhibit much more intensity, implying that the six peaks consist of adducts of DMPO-RI and DMPO-RII. Consequently, on the basis of the results and the reactive species involved in the process, it can be stated that RI and RII are formed in dehydrogenation and hydrogenolysis reactions.

It should be noted that, according to theoretical analysis, the yield of pMA should be equal to that of pMBAD. However, the yield of pMA is always slightly lower than that of pMBAD (for instance, after light irradiation for 4 h, the yields of pMA and pMBAD are 41.7% and 52.3%, respectively). In the previous report [23], besides toluene, H₂ was also formed by the dehydrogenation of benzyl alcohol (H₂ effect), meaning that the dehydrogenation of benzyl alcohol is a competitive process. To make it clear in our reaction system, the headspace of the reactor was analyzed, and the results showed that no H₂ were detected after irradiation for 4 h. However, considerable H₂ was measured when the reaction system was conducted on a H₂ evolution reaction system (Fig. S15). Moreover, the apparent reaction rate constant is 0.5302 h⁻¹, and the yield of pMA is much less than that of pMBAD. These results indicate that the dehydrogenation of benzyl alcohol is indeed a competitive process. Atmospheric pressure favors hydrogenolysis of pMBA into pMA, whereas vacuum favors formation of H₂. Therefore, a reasonable explanation (for why the yield of pMA is always slightly less than that of pMBAD) is that H₂ is indeed produced but in very small concentrations under 0.1 MPa N₂. Thus, H₂ is dis-

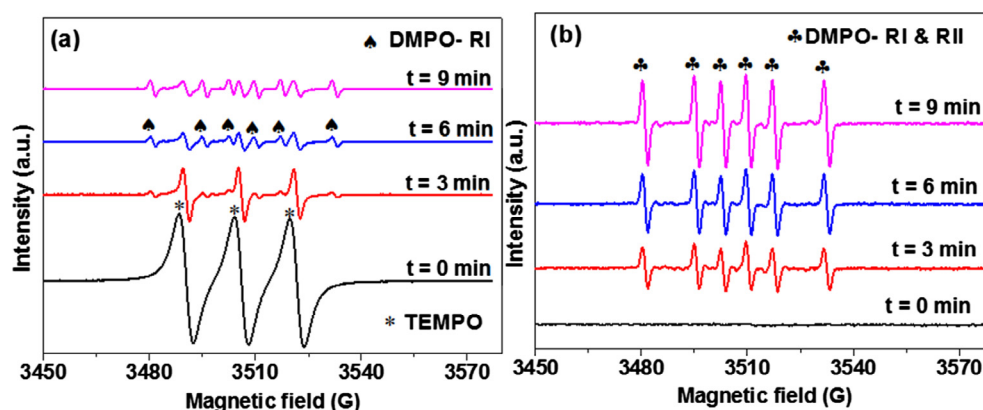


Fig. 8. EPR spectra of the photocatalytic redox reaction system in presence of (a) DMPO and TEMPO and (b) only DMPO registered after different irradiation times.

solved in the solvent. It does not desorb until the pressure of the system is reduced (vacuum) to extract it. These results also reveal that CdS-Hy or other photocatalysts may be used for dehydrogenation of aromatic alcohols to aromatic aldehydes and renewable fuels (such as H₂) in one reaction system.

4. Conclusions

In summary, we have demonstrated that the band potentials of semiconductors and charge separation–transportation are two crucial factors for photocatalysts suitable for visible-light photoredox catalysis. The optimum positions are that the valence band position should be located between the oxidation potentials of p-methoxybenzyl alcohol/p-methoxybenzaldehyde and p-methoxybenzaldehyde/oxidized p-methoxybenzaldehyde, and the conduction band position should be slightly more negative than the reduction potential of p-methyl anisole/p-methoxybenzyl alcohol. Dispersed CdS nanoparticles synthesized by a simple hydrothermal method could selectively and efficiently photocatalyze dehydrogenation and hydrogenolysis of aromatic alcohols in one reaction system under visible light and mild conditions. In the cooperative photoredox reaction, dehydrogenation consumes two holes and produces two protons; hydrogenolysis depletes two electrons and two protons. In this process, photogenerated holes and electrons are directly utilized by dehydrogenation and hydrogenolysis to form corresponding alkanes/ethers and aldehydes, respectively. This synergetic system is favorable to improving the separation efficiency of photogenerated electron–hole pairs. Thus, the reaction system contributes to the improvement of photocatalytic activity and stability. This work is of great value to the application and efficient use of solar energy in practice. We hope that this work will expand the range of highly efficient, visible-light-driven photocatalysts available for selective transformations of organics under ambient conditions.

Acknowledgments

This work was financially supported by the National Natural Science Foundation of China (NSFC, Grants 51472005, 51772118, and 21473066) and the Natural Science Foundation of Anhui Province, China (Grants 1408085QB38 and 1608085QB37).

Appendix A. Supplementary material

Supplementary data associated with this article can be found, in the online version, at <https://doi.org/10.1016/j.jcat.2017.11.015>.

References

- [1] K.K. Sakimoto, A.B. Wong, P. Yang, *Science* 351 (2016) 74–77.
- [2] K.A. Brown, D.F. Harris, M.B. Wilker, A. Rasmussen, N. Khadka, H. Hamby, S. Keable, G. Dukovic, J.W. Peters, L.C. Seefeldt, P.W. King, *Science* 352 (2016) 448–450.
- [3] C. Huang, C. Chen, M. Zhang, L. Lin, X. Ye, S. Lin, M. Antonietti, X. Wang, *Nat. Commun.* 6 (2015) 7698.
- [4] N. Zhang, M. Yang, Z. Tang, Y. Xu, *J. Catal.* 303 (2013) 60–69.
- [5] N. Zhang, M. Yang, S. Liu, Y. Sun, Y. Xu, *Chem. Rev.* 115 (2015) 10307–10377.
- [6] X. Lang, J. Zhao, X. Chen, *Angew. Chem. Int. Ed.* 55 (2016) 4697–4700.
- [7] X. Lang, J. Zhao, X. Chen, *Chem. Soc. Rev.* 45 (2016) 3026–3038.
- [8] J.C. Colmenares, R. Luque, *Chem. Soc. Rev.* 43 (2014) 765–778.
- [9] G. Palmisano, V. Augugliaro, M. Pagliaro, L. Palmisano, *Chem. Commun.* 33 (2007) 3425–3437.
- [10] A. Maldotti, A. Molinari, R. Amadelli, *Chem. Rev.* 102 (2002) 3811–3836.
- [11] M. Zhang, Q. Wang, C. Chen, L. Zang, W. Ma, J. Zhao, *Angew. Chem. Int. Ed.* 48 (2009) 6081–6084.
- [12] S. Yurdakal, G. Palmisano, V. Loddo, V. Augugliaro, L. Palmisano, *J. Am. Chem. Soc.* 130 (2008) 1568–1569.
- [13] X. Lang, X. Chen, J. Zhao, *Chem. Soc. Rev.* 43 (2014) 473–486.
- [14] T. Mallat, A. Baiker, *Chem. Rev.* 104 (2004) 3037–3058.
- [15] L. Zhao, Q. Meng, X. Fan, C. Ye, X. Li, B. Chen, V. Ramamurthy, C. Tung, L. Wu, *Angew. Chem. Int. Ed.* 56 (2017) 3020–3024.
- [16] Z. Chai, T. Zeng, Q. Li, L. Lu, W. Xiao, D. Xu, *J. Am. Chem. Soc.* 138 (2016) 10128–10131.
- [17] N. Zhang, Y. Zhang, M. Yang, Z. Tang, Y. Xu, *J. Catal.* 299 (2013) 210–221.
- [18] H. Li, F. Qin, Z. Yang, X. Cui, J. Wang, L. Zhang, *J. Am. Chem. Soc.* 139 (2017) 3513–3521.
- [19] B. Zhang, J. Li, Y. Gao, R. Chong, Z. Wang, L. Guo, X. Zhang, C. Li, *J. Catal.* 345 (2017) 96–103.
- [20] J. Wan, X. Du, E. Liu, Y. Hu, J. Fan, X. Hu, *J. Catal.* 345 (2017) 281–294.
- [21] X. Ning, S. Meng, X. Fu, X. Ye, S. Chen, *Green Chem.* 18 (2016) 3628–3639.
- [22] C. Ling, X. Ye, J. Zhang, J. Zhang, S. Zhang, S. Meng, X. Fu, S. Chen, *Sci. Rep.* 7 (2017) 27.
- [23] T.P.A. Ruberu, N.C. Nelson, I.I. Slowing, J. Vela, *J. Phys. Chem. Lett.* 3 (2012) 2798–2802.
- [24] W. Adam, C.R. Saha-Möllner, P.A. Ganeshpуре, *Chem. Rev.* 101 (2001) 3499–3548.
- [25] R.A. Sheldon, I.W.C.E. Arends, G.J. Ten Brink, A. Dijkman, *Acc. Chem. Res.* 35 (2002) 774–781.
- [26] M. Sun, D. Li, W. Li, Y. Chen, Z. Chen, Y. He, X. Fu, *J. Phys. Chem. C* 112 (2008) 18076–18081.
- [27] T. Tachikawa, Y. Takai, S. Tojo, M. Fujitsuka, H. Irie, K. Hashimoto, T. Majima, *J. Phys. Chem. B* 110 (2006) 13158–13165.
- [28] J. Zhang, S. Meng, X. Ye, C. Ling, S. Zhang, X. Fu, S. Chen, *Appl. Catal. B Environ.* 218 (2017) 420–429.
- [29] S. Chen, H. Zhang, X. Fu, Y. Hu, *Appl. Surf. Sci.* 275 (2013) 335–341.
- [30] J. Liu, T. Zhang, Z. Wang, G. Dawson, W. Chen, *J. Mater. Chem.* 21 (2011) 14398–14401.
- [31] J. Zhang, Y. Hu, X. Jiang, S. Chen, S. Meng, X. Fu, *J. Hazard. Mater.* 280 (2014) 713–722.
- [32] D. Wang, L. Wang, A. Xu, *Nanoscale* 4 (2012) 2046–2053.
- [33] H. Zhao, Y. Dong, P. Jiang, G. Wang, H. Miao, R. Wu, L. Kong, J. Zhang, C. Zhang, *A.C.S. Sust. Chem. Eng.* 3 (2015) 969–977.
- [34] Q. Wang, J. Li, Y. Bai, J. Lian, H. Huang, Z. Li, Z. Lei, W. Shangguan, *Green Chem.* 16 (2014) 2728–2735.
- [35] P. Zhou, J. Yu, M. Jaroniec, *Adv. Mater.* 26 (2014) 4920–4935.
- [36] X. Xiao, J. Jiang, L. Zhang, *Appl. Catal. B Environ.* 142 (2013) 487–493.
- [37] F. Xiao, J. Miao, B. Liu, *J. Am. Chem. Soc.* 136 (2014) 1559–1569.
- [38] M. Yang, C. Han, N. Zhang, Y. Xu, *Nanoscale* 7 (2015) 18062–18070.
- [39] B.L. He, B. Dong, H.L. Li, *Electrochem. Commun.* 9 (2007) 425–430.
- [40] H. Zhang, X.J. Lv, Y.M. Li, Y. Wang, J.H. Li, *ACS Nano* 4 (2010) 380–386.
- [41] F. Xiao, S. Hung, J. Miao, H. Wang, H. Yang, B. Liu, *Small* 11 (2015) 554–567.
- [42] C. Xu, P.H. Shin, L. Cao, J. Wu, D. Gao, *Chem. Mater.* 22 (2010) 143–148.
- [43] A. Zaban, M. Greenshtein, J. Bisquert, *ChemPhysChem* 4 (2003) 859–864.
- [44] X.H. Li, X. Wang, M. Antonietti, *Chem. Sci.* 3 (2012) 2170–2174.
- [45] J. Yang, H. Yan, X. Wang, F. Wen, Z. Wang, D. Fan, J. Shi, C. Li, *J. Catal.* 290 (2012) 151–157.
- [46] J.E. Chateaufneuf, *J. Am. Chem. Soc.* 112 (1990) 442–444.
- [47] W. Choi, M.R. Hoffmann, *Environ. Sci. Technol.* 29 (1995) 1646–1654.
- [48] X. Wang, K. Maeda, A. Thomas, K. Takanabe, G. Xin, J.M. Carlsson, K. Domen, M. Antonietti, *Nat. Mater.* 8 (2009) 76–80.
- [49] G. Ma, H. Yan, J. Shi, X. Zong, Z. Lei, C. Li, *J. Catal.* 260 (2008) 134–140.
- [50] D. Ma, A. Liu, C. Lu, C. Chen, *ACS Omega* 2 (2017) 4161–4172.
- [51] M. Zhang, C. Chen, W. Ma, J. Zhao, *Angew. Chem. Int. Ed.* 120 (2008) 9876–9879.
- [52] B.K. Sinha, *Biochem. Pharmacol.* 33 (1984) 2777–2781.
- [53] L. Wang, X. Wei, W. Jia, J. Zhong, L. Wu, Q. Liu, *Org. Lett.* 16 (2014) 5842–5845.
- [54] W. He, H. Kim, W.G. Wamer, D. Melka, J.H. Callahan, J. Yin, *J. Am. Chem. Soc.* 136 (2013) 750–757.